Available online at www.sciencedirect.com
ScienceDirect
Journal of Power Sources 162 (2006) 286–293
JOURNAL OF POWER SOURCES
www.elsevier.com/locate/jpowsour

Spatially resolved optical measurements of water partial pressure and temperature in a PEM fuel cell under dynamic operating conditions

S. Basu, M.W. Renfro, B.M. Cetegen *

Mechanical Engineering Department, University of Connecticut, 191 Auditorium Road, U-3139, Storrs, CT 06269-3139, United States

Received 19 May 2006; received in revised form 22 June 2006; accepted 23 June 2006
Available online 1 August 2006

Abstract

In situ non-intrusive measurements of water vapor partial pressure and temperature were performed simultaneously along two gas channels on the cathode side of a PEM fuel cell using tunable diode laser absorption spectroscopy. This measurement technique developed by us was utilized earlier to make measurements in a single bipolar plate channel of a prototype PEM fuel cell. The current study examines the variation of water partial pressure and temperature near the flow inlet and outlet during operation under both steady state and time-varying load conditions. For steady-state operation, an increase in the water vapor partial pressure was observed with increasing current density due to electrochemical production of water. As expected, the measurement channel near the inlet of the flow path showed a lower water vapor partial pressure than the outlet under identical load conditions; however, the quantitative distribution of water content across the cell is important to understanding operational behavior of a PEM fuel cell. These quantitative water concentration differences between two measurement channels are reported with variations in cell load and temperature. Temperature in the gas phase remained constant due to thermal equilibrium of the fuel cell. For time varying operation, no phase lag was observed between the load and the water vapor partial pressure. The outlet measurement channel showed higher partial pressure than the inlet with larger differences for increasing cell load. The transient data matched the steady-state measurements at the same conditions. A temperature rise from the controlled value was observed at high current densities for the unsteady operation; thus, the temperature did not equilibrate on the same time scale as the water partial pressure.

Keywords: Optical diagnostics; PEM fuel cell testing; Laser absorption; Water vapor concentration; Temperature

1. Introduction

Performance in proton exchange membrane (PEM) fuel cells is strongly affected by the transport processes that occur both across the thin membrane separating the fuel and oxidizer streams and in the plane of the gas flows through the bipolar plate [1,2]. Prior research has shown that the most common Nafion© membrane used in PEM fuel cells exhibits a protonic conductivity increase by an order of magnitude when the relative humidity of the gas streams change from 35 to 85% [3]. For this and other reasons, water management in PEM fuel cells is an important element in optimization of transport across the membrane, and therefore overall system performance.

Although air and fuel gas (typically hydrogen) with controlled levels of humidification are fed into the flow channels in the bipolar plates surrounding the membrane-electrode assembly (MEA), the complex water transport mechanisms in the stack and across the membrane can lead to highly inhomogeneous water distributions. The water distribution is affected by the water generation at the cathode due to electrochemical reaction, the electro-osmotic drag that is responsible for water transport from anode to cathode side, and the diffusion of water from cathode to anode [1,2,4]. In addition, as hydrogen and oxidizer are consumed in the gas flows through the bipolar plates, the concentrations of the reactants change and the boundary conditions for transport across the membrane are altered. As a result, there can be substantial variation of water concentration in the flow channels of the bipolar plate, which may lead to local drying or flooding of the membrane, local variations in temperature, and consequently negatively affect the performance of a PEM fuel cell. These spatial inhomogeneities may be further accentuated by dynamic loading of a PEM fuel cell since the time scales for transport within the bipolar plates and across the membrane will not necessarily be equal. For these reasons, understanding of

* Corresponding author. Tel.: +1 860 486 2966; fax: +1 860 486 5088.
E-mail address: cetegen@engr.uconn.edu (B.M. Cetegen).

0378-7753/$ – see front matter © 2006 Elsevier B.V. All rights reserved.
doi:10.1016/j.jpowsour.2006.06.073

the distribution of water and local temperatures within operating fuel cells is important for optimization of fuel cell design and operation. Accurate, fast, in situ measurements of water vapor concentration and temperatures within the cell enable both better understanding of water transport for improved cell design and implementation of advanced control strategies.

Development of non-intrusive diagnostics for sensing of temperature and gas species in fuel cells is relatively new with most measurements in fuel cell systems limited to global inlet and outlet measurements. Water measurements have been performed by chilled water hygrometry [5], gas chromatography [6,7] and Fourier transform infrared (FT-IR) spectroscopy [8]. If implemented for in-cell measurements, these techniques become intrusive since they require extraction of gas samples from the cell. Additionally, imaging techniques such as neutron scattering [9,10] and X-ray scattering [11] have been utilized for determining the spatial distribution of hydration states. However, such techniques require placement of the fuel cell in sophisticated large-scale instruments that are not widely available. To overcome these limitations, a non-intrusive measurement technique was developed [12,13] to permit local measurements of gas composition and temperature within a PEM cell. This technique utilizes tunable diode laser absorption spectroscopy (TDLAS), and has been applied to measurements of water vapor concentration [12] and gas temperature [13] along a single line-of-sight within a modified optically accessible fuel cell. The measurement technique provides good temporal resolution and can be integrated into operating fuel cell stacks with minimal modification. The spatial resolution of the instrument resolves path-integrated values for one channel across a bipolar plate. In a typically serpentine geometry, this path average represents a measurement over a relatively small fraction of the total flow path. Previously, measurements were performed for both steady state and a particular transient operation of a PEM fuel cell in a single flow channel.

In this article, the TDLAS measurement technique [12,13] is applied to measure the water vapor concentration and temperature simultaneously in two flow channels in the bipolar plate of a prototype PEM fuel cell employing a serpentine flow geometry. In this way, spatial variations in the plane of the bipolar plate can be directly recovered using a non-intrusive measurement technique. In-plane variations of water concentration can be used to indicate non-homogeneous water transport or production. A quantitative measurement of the difference in water content across the cell may be useful for identifying problem locations in a membrane or cell design. Experiments in this paper include both steady state and transient operation of the fuel cell with a sinusoidal time varying current. The rate of the sinusoidal variations is altered to examine the combined spatial and temporal response of water transport in the fuel cell.

2. Experimental approach

The experimental methodology is based on that previously reported by Basu et al. [12,13], and is briefly reviewed here. Tunable diode laser absorption spectroscopy was used to measure water vapor absorption profiles as a function of excitation wavelength. Two channels of the serpentine flow path of a bipolar plate were slightly modified for optical access. The bipolar plate included a total of 17 flow channels in a serpentine geometry of which the 3rd and 12th channels from the inlet on the cathode side were selected for the measurements. Each flow channel length was 7 cm with channel cross sectional dimensions of 1.5 mm × 2.0 mm as schematically shown in Fig. 1. For optical access, the two selected channels were milled out to the end of the bipolar plate so that the diode laser beam could be transmitted along the channel length. The recovered measurements represent a path average along this channel, which include only 5.8% of the total flow path.

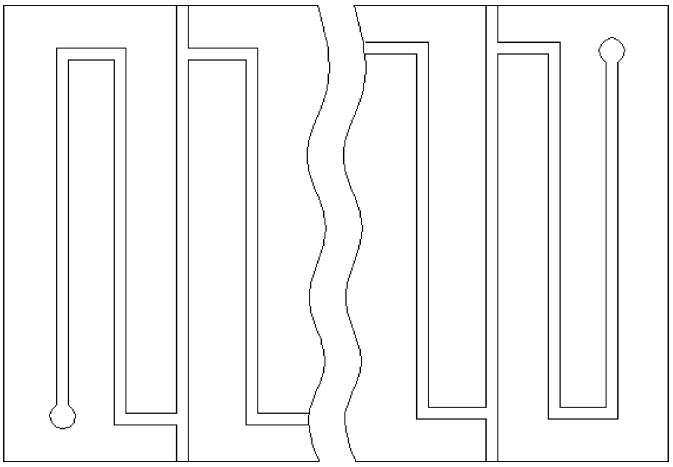

Fig. 1. Schematic of the bipolar plate. The 3rd (near the inlet) and 12th (near the outlet) channels are extended to the edges of the plate for optical access.

To enable measurements across both channels simultaneously, the pigtailed output of a distributed feedback (DFB) diode laser at a wavelength of 1470 nm was split using a bifurcated 2 × 2 optical fiber. One leg of the fiber was fed to a reference photodiode for measuring the laser power without absorption while the other leg was fed into another 2 × 2 bifurcated optical fiber. The output legs of this fiber were attached to two beam collimating lenses and placed at the ends of the milled flow channels. The collimating lenses served the dual purpose of sealing the ends of the channels as well as focusing the laser beam to a spot size of about 1 mm. This was essential for aligning the beam in the narrow, long channels with an aspect ratio of about 100.

The wavelength of the DFB diode laser was tuned by temperature and current control. A thermoelectric temperature controller (Thorlabs TEC2000) was used to provide coarse adjustment of the laser wavelength. Rapid tuning of the laser wavelength was achieved by ramping the laser current input using a current controller (Thorlabs LDC5000) as shown in Fig. 2. The current ramp function was generated by the data acquisition computer at a frequency of 50 Hz allowing the laser wavelength to scan 0.15 nm around the 1470 nm transition. The laser wavelength was calibrated using an optical spectrum analyzer, and the wavelength change during the rapid scan was monitored by a ring interferometer. Since both laser power and its emission wavelength change during the current ramp, a reference photodiode, PD1 in Fig. 2

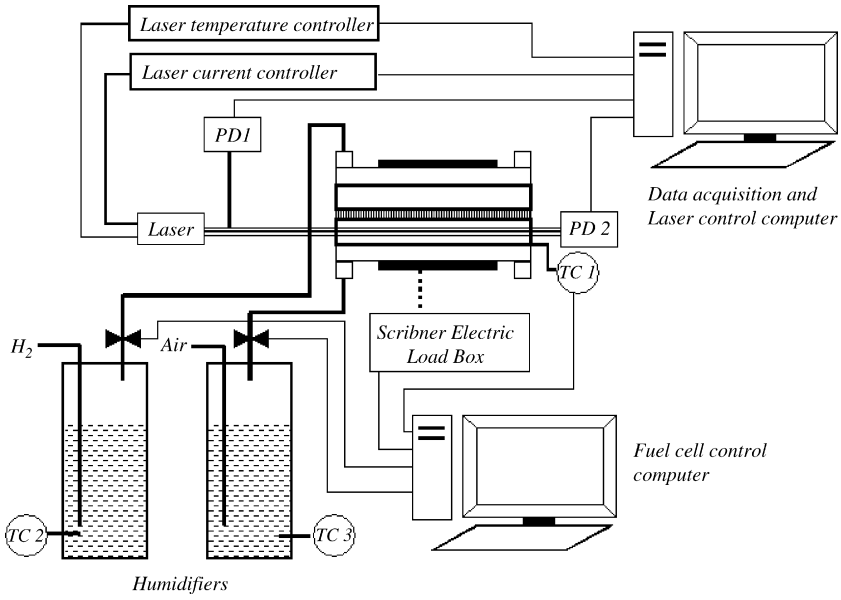

Fig. 2. Experimental set-up for calibration, steady state and dynamic tests. Thermocouples (TC) are used to control the humidity of the cell.

(Thorlabs PDA400), was used to monitor the laser power prior to entering the fuel cell. The attenuated laser signal was measured by two photodetectors, PD2 in Fig. 2 (Thorlabs PDA400), at the opposite ends of the modified fuel cell gas channels. The attenuated signals include the absorption by water and any non-resonant losses. The peak laser absorption was typically around 2% for the conditions examined in this study.

The membrane electrode assembly utilized in this study contained Perfluorosulfonic acid (PSA) polymer membrane made by 3M Corporation (product ID: 98-0001-0134-9). The hydrogen and air streams fed into the fuel cell were humidified by passing them through a temperature controlled water bath prior to entering the fuel cell. Further heating of the gases, and electrical heating pads on the fuel cell surface were used to provide independent control of gas temperature, humidity, and cell temperature. The humidifier outlet streams were saturated within 1% at the humidifier exit temperature. The external electrical load on the fuel cell was controlled by a Scribner 890CL fuel cell testing load box.

The calibration of the TDLAS measurement system was performed by feeding only the cathode side of the fuel cell with air of known humidity. The flow on the anode side was blocked to prevent any electrochemical reaction from producing water in the cathode channel. The cell was held at a fixed temperature using a temperature controller during the calibration and during the fuel cell experiments. In an earlier study, Basu et al. [12] showed that the water transitions in the vicinity of 1491 nm were significantly stronger than the transitions near 1470 nm, but they were only sensitive to partial pressure and not temperature. Some measurements were carried out in this study at 1491 nm for comparison to the results at 1470 nm. However, all temperature measurements were performed using the 1470 nm transition.

The absorption of the laser beam passing through the gas sample is related to the water vapor partial pressure, P_v (atm), of the absorbing species by Beer's law [14]:

$$\frac{I}{I_0} = \exp\left(-\int_0^L \kappa P_v \, dl\right) \quad (1)$$

where κ (atm^{-1} cm^{-1}) is the wavelength and temperature dependent absorption coefficient, I is the measured intensity of the laser leaving the channel from PD2, and I_0 is the laser intensity without absorption from PD1. The integration is performed over the path length L of the gas sample, in this case over the 7-cm channel length. The absorption coefficient displays strong peaks as a function of wavelength due to the discrete rotational and vibrational energy transitions of the water molecule. The absorption coefficient is also temperature dependent since the distribution of water molecules among its various energy levels depends on temperature. In the experiment, the absorption signal is monitored using the data acquisition computer during the repeated current ramps to the laser. The absorption variations in time can then be related to the laser wavelength thereby generating a spectral absorption profile. During each current ramp, 2000 data points were acquired at a sampling frequency of 100 kHz. The profiles were averaged over 200 separate scans resulting in a temporal resolution of 4 s.

2.1. Spectral characteristics of water

In the spectral region spanned by the laser, five transitions contribute to the overall measured absorption profile. The data analysis consists of a non-linear curve fit algorithm described by Basu et al. [12,13] to determine the width and peak of each transition. As shown previously, water–water collisions are very effective in broadening the water absorption profiles (compared to water–air collisions). Thus, the spectral width of the measured TDLAS profile changes substantially with water partial pressure, and temperature has minimal impact on the width

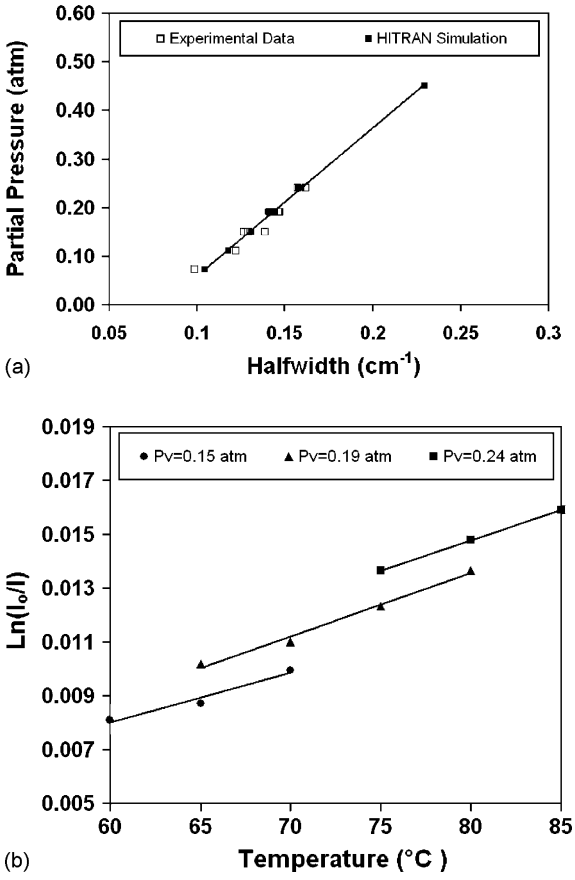

Fig. 3. Calibration of (a) partial pressure vs. half-width calibration and (b) peak absorption intensity vs. temperature at different water partial pressures (P_v). The predicted relationship between partial pressure and half-width is also shown in (a) using the HITRAN absorption database.

[12]. Temperature on the other hand is obtained from measuring the peak intensity of water absorption. In this manner, water partial pressure and temperature can be simultaneously determined using the water absorption spectral shape and strength for transitions in the range of 1470.30–1470.42 nm. Based on this approach, Fig. 3 shows the resulting calibration curves for partial pressure and temperature. The partial pressure of water is first determined from the width of the absorption profile (Fig. 3(a)) and then the peak intensity is used to determine the temperature (Fig. 3(b)). The water partial pressure can be determined with an accuracy ±5% and the temperature can be determined with an accuracy ±2 °C within the temperature measurement range of 60–85 °C. Further details of the calibration and measurement analysis can be found in Basu et al. [13].

3. Results and discussion

In this section, the water vapor partial pressure and temperature measurements made in two channels of a serpentine flow geometry of a single PEM fuel cell are reported. The measurements were made under steady state as well as sinusoidal time varying current conditions at two oscillation frequencies. The steady-state measurements are first discussed with emphasis on the spatial variations of the measurements. This is followed by

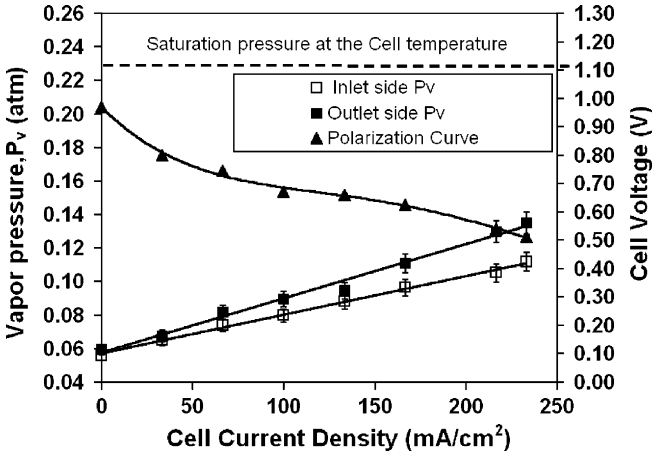

Fig. 4. Variation of steady-state partial pressure with applied load for the two channels. Inlet partial pressure is 0.054 atm. The polarization curve (voltage) of the cell during loading is also shown.

the presentation of the results for time varying current profiles and the effects of unsteady operation on the water vapor partial pressure and gas temperatures.

3.1. Measurements at steady-state fuel cell operation

Fig. 4 shows the partial pressure variation across the two channels, one near the inlet and the other near the outlet of the serpentine bipolar plate geometry shown in Fig. 1 as a function of operating current density. In this case, the inlet water vapor partial pressure was 0.054 atm with the cell operating temperature of 65 °C corresponding to an inlet relative humidity of 22.6%. As shown in previous measurements, the water partial pressure on the cathode side increases linearly with the current density [12]. As more current is drawn from the cell, the combined effects of water production on the cathode side and other water transport effects such as electro-osmotic drag from anode to cathode are responsible for the measured differences. It is seen in this figure that the water partial pressure is always higher in the outlet measurement channel than the inlet channel in this serpentine flow geometry. The difference in water vapor partial pressure increases with increasing current density. The partial pressure difference between outlet and inlet channels is very small at low current settings below 30 mA cm^{-2} and grows to 0.024 atm at the current setting of 233 mA cm^{-2}.

Fig. 5 shows the partial pressure variation for a higher inlet water vapor partial pressure of 0.22 atm and cell operating temperature of 85 °C, with a corresponding relative humidity of 40%. The measurements show again that the partial pressure increases linearly with current density. The rate of increase, $\Delta P_v/\Delta I$, is approximately 0.00030 atm cm^2 mA^{-1} for the inlet channel and 0.00037 atm cm^2 mA^{-1} for the outlet channel. These values compare with 0.00023 atm cm^2 mA^{-1} for the inlet channel and 0.00032 atm cm^2 mA^{-1} for the outlet channel for the experimental conditions of Fig. 4.

Water production and electro-osmotic drag increase with cell current resulting in high water content on the cathode side of the fuel cell at high current densities. However, these spatially

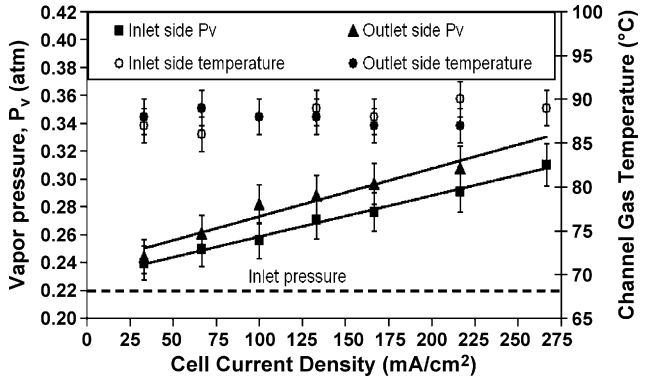

Fig. 5. Variation of steady-state partial pressure and temperature with applied load for the two channels. Inlet partial pressure is 0.22 atm.

resolved measurements show that water transport within the flow passages of the bipolar plate via advection is not fast enough to equilibrate the water content in the plane of the bipolar plate. The differences in the slopes of the water partial pressure curves versus current detail the level of non-homogeneous conditions present in the fuel cell. For the lower temperature operating conditions, the spatial inhomogeneity from inlet to outlet is 24% of the average water partial pressure and for the higher temperature operating conditions is 9% of the average water partial pressure. This difference can be explained by the fact that at the higher inlet humidity levels afforded by higher cell temperature, advection of water through the bipolar plate flow passages is a larger contributor to overall water transport and causes more uniform conditions. Whereas, at low inlet humidity, most of the water in the cathode flow passage comes from the membrane (via production or electro-osmotic drag) and builds up from inlet to outlet.

To provide further insight into the water transport occurring in this particular cell, Fig. 6 shows the expected water partial pressure increase as a function of cell current density assuming that water is produced homogeneously at a rate governed by the cell's overall measured current. The calculated results are compared to the experimental data at two different fuel cell operating conditions. Calculated water production due to electrochemical reaction fully accounts for the measured water partial pressure difference between inlet and outlet, indicating that water transport by electro-osmotic drag does not contribute appreciably to this increase. This is consistent with the observation that water partial pressure increases linearly with current under all conditions examined here. Thus, electro-osmotic drag is not significant at these conditions.

The path-averaged gas temperatures were also measured using the 1470 nm transition and are shown in Fig. 5. The temperature shows a variation between 85 and 90 °C over the whole current range; however there is no systematic temperature variation greater than the uncertainty in the measurement (±2 °C). It should be noted that the temperature of the cell is controlled by a temperature controller at 85 °C, and the cell is allowed to fully reach steady state with each discrete increase in cell current. Thus, larger changes in temperature may not be expected based on the thermal equilibrium of the cell.

3.2. Measurements during dynamic fuel cell operation

Fig. 7 shows the water partial pressure obtained during a dynamic current cycle with peak amplitude of 130 mA cm^{-2} at a frequency of 1/120 Hz. During these measurements, the fuel cell was kept at a particular current setting for about 12 s. The data collection started one second after each current setting and continued for 4 s during which 300 laser scans were obtained. For an inlet water vapor partial pressure of 0.05 atm, the partial pressure variation in the cell closely follows the current cycle without any detectable phase lag. The partial pressure rises to a maximum of 0.1 atm for a peak current value of 130 mA cm^{-2} and reduces to a minimum value of about 0.052 atm at zero current. The partial pressure variation across two current cycles is repeatable showing the outlet channel having a higher water vapor partial pressure than the inlet channel, as with the steady-state results. The difference between the outlet and the inlet channel partial pressures is highest at the peak current. The transient data match well with the steady-state measurements, indicating that the time scale of equilibration is smaller than the time scale of the measurement ($\tau = 4$ s).

Fig. 8(a) and (b) illustrate the partial pressure variation at a cell temperature of 65 °C and inlet water partial pressure of 0.05 atm for two current cycles of the same current amplitude

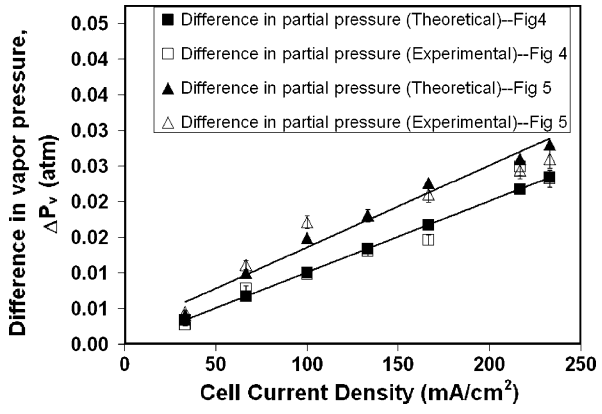

Fig. 6. Comparison of calculated and measured difference in water partial pressure between the inlet and outlet channels. Experimental conditions are the same as those in Figs. 4 and 5.

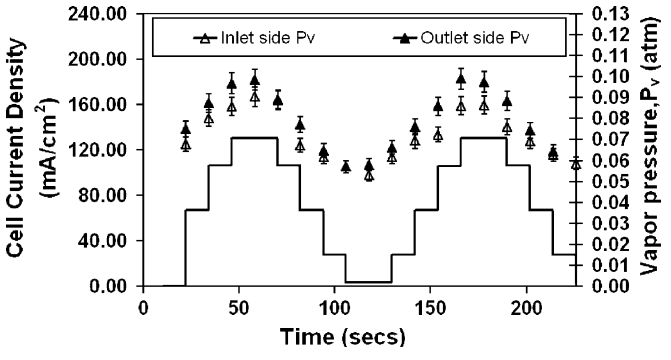

Fig. 7. Variation of partial pressure with dynamic load for the two channels. Inlet partial pressure is 0.05 atm.

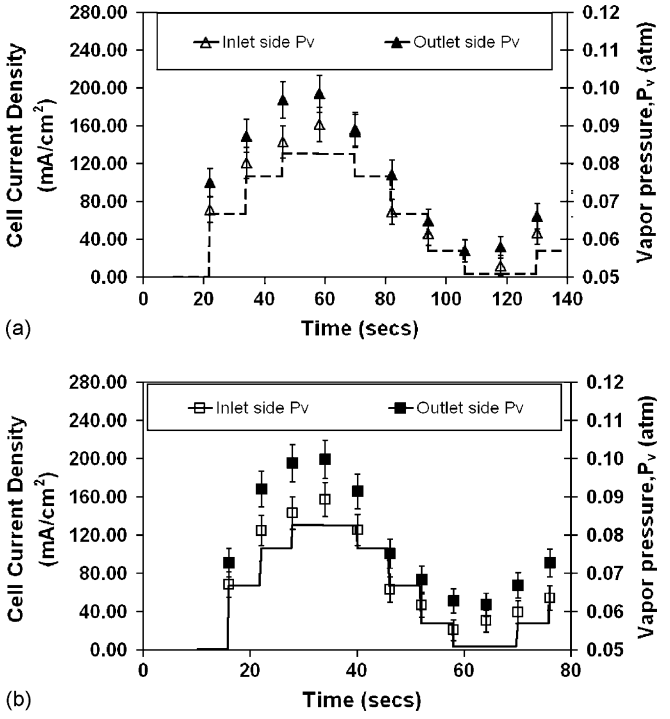

Fig. 8. Variation of partial pressure with dynamic loads of (a) low frequency and (b) high frequency for the two channels. The operating conditions of the cell are the same for both frequencies. Inlet partial pressure is 0.05 atm and the cell nominal temperature is 65 °C.

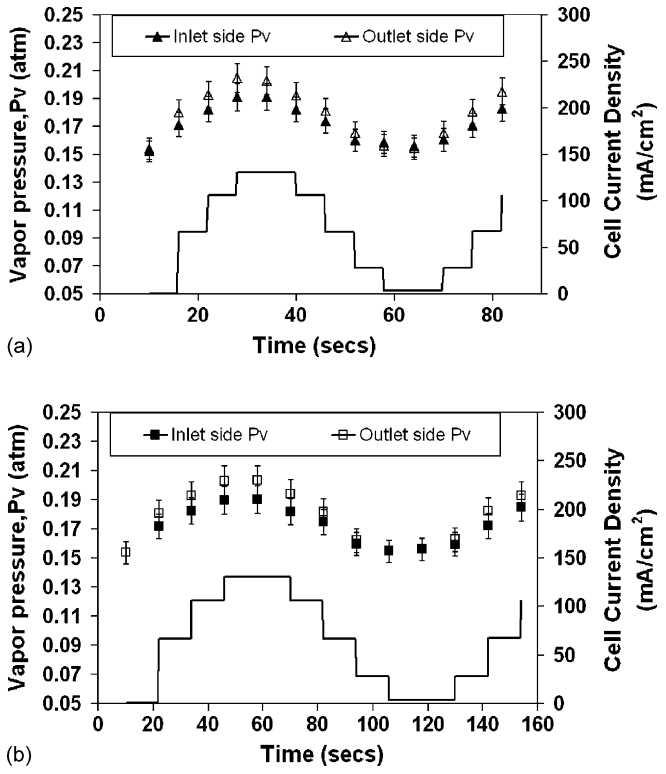

Fig. 9. Variation of partial pressure with dynamic loads of (a) low frequency and (b) high frequency for the two channels. The operating conditions of the cell are the same for both frequencies. Inlet partial pressure is 0.15 atm and the cell nominal temperature is 81 °C.

but at two different frequencies (f = 1/120, 1/60 Hz) for the same set of operating conditions as in Fig. 7. The measurements and comparisons are shown for one cycle only as the cycles are highly repeatable. Similar to the low frequency case (Fig. 8(a)), the water vapor partial pressure for the high frequency case (Fig. 8(b)) also follows the current variation without any phase lag. The partial pressure difference between the inlet and outlet channels is maintained throughout the cycle with a slightly smaller difference when the cell is unloaded. For the higher frequency, each current setting has a transient duration of 6 s with the measurement being performed from 1 to 5 s during this period. The partial pressure variations are almost identical to one another with very little dependence on the frequency of the current cycle.

Fig. 9(a) and (b) illustrate the water vapor partial pressure for an inlet partial pressure of 0.15 atm and a cell temperature of 81 °C during two different loading frequencies. The partial pressure difference between the outlet and inlet channels for both frequencies is highest at the peak current and gradually diminishes as the current is reduced. Both the channels attain the water partial pressure of the inlet stream at zero loading. Again as observed in Fig. 8, no influence of the current cycle frequency is detected on the variation of the partial pressure. At least for these relatively slow cycles (maximum f = 1/60 Hz), the water partial pressure equilibrates within the time scale of measurement (4 s).

Fig. 10 illustrates the temperature measurements for the same set of experimental conditions as in Fig. 9 for two different load frequencies. It is observed in Fig. 10(a) for the low frequency

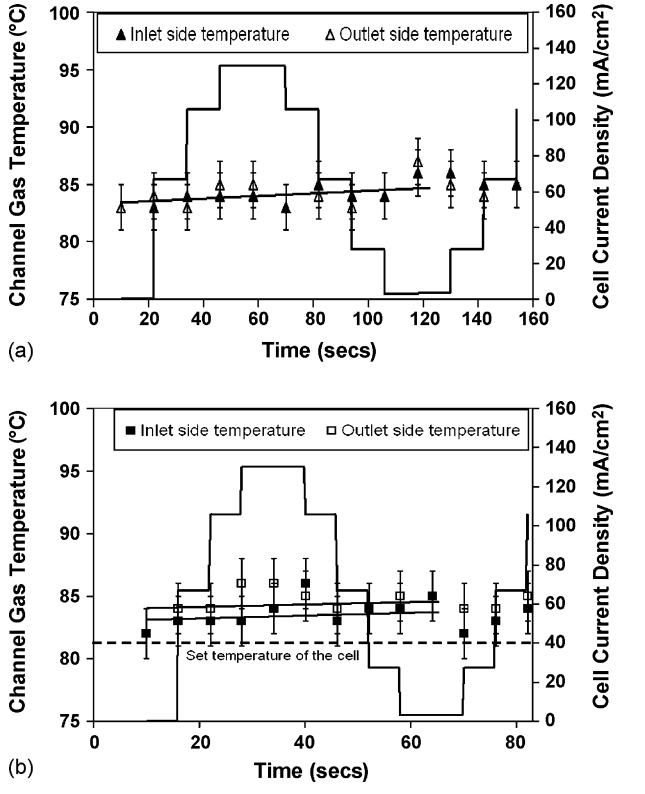

Fig. 10. Variation of temperature with dynamic loads of (a) low frequency and (b) high frequency for the two channels. The operating conditions of the cell are the same for both frequencies. Inlet partial pressure is 0.15 atm and the cell nominal temperature is 81 °C.

cycle that the temperature is equal for the inlet and outlet channels but is not constant with cell current, as in the steady-state measurements of Fig. 5. As the current increases, the cell temperature increases above the control value. This was also observed in the previously reported measurements [13]. The time scale for the cell temperature to re-equilibrate is longer than the dynamic loading time as evidenced by the fact that the temperature does not follow a sinusoidal variation, but gradually increases. This behavior suggests that the local gas temperature increases from the nominal value with time varying current in spite of having an external control on the temperature of the cell. Although the gas temperature rises during the peak load, no temperature drop is observed during reduction of the cell current. This thermal behavior can be rationalized based on the larger thermal inertia of the cell and the consequently slower time response.

For the high frequency cycle (Fig. 10(b)), the temperatures in both channels again increase throughout the cycle. However, the outlet side channel shows a higher average value than the inlet side channel. The temperature difference between the channels is the highest when the partial pressure difference (Fig. 9(a)) is the maximum. Temperature variations of 4–5 °C are observed particularly in the outlet channel. Although the typical error in the temperature measurement is ±2 °C, the rise in temperature from the nominal value of 81 °C is significant. Also the temperature does not undergo cyclic variations like partial pressure because of the external control and the large thermal inertia of the cell.

Fig. 11 shows the partial pressure and temperature variation for an inlet partial pressure of 0.05 atm, a cell temperature of 65 °C and current amplitude of 260 mA cm^{-2}. Here, the current amplitude is twice the amplitude reported in the earlier results, and the inlet gas flows are less humid. Fig. 11(a) shows, in comparison with Fig. 8(a), that the difference of the water partial pressures is significantly higher at the peak current value of 260 mA cm^{-2} than at the current value of 130 mA cm^{-2}. Apart from the larger peak difference in partial pressure values, the profiles are qualitatively similar to those shown for the lower peak current amplitude. Fig. 11(b) shows the temperature variation for the higher current amplitude. The temperature variation exhibits an increase with time with the highest temperature reaching 72 °C. Hence compared with a lower amplitude variation like Fig. 10(b), a more pronounced temperature non-equilibrium exists for both the channels; although there is no detectable temperature difference across the channels for the higher amplitude case.

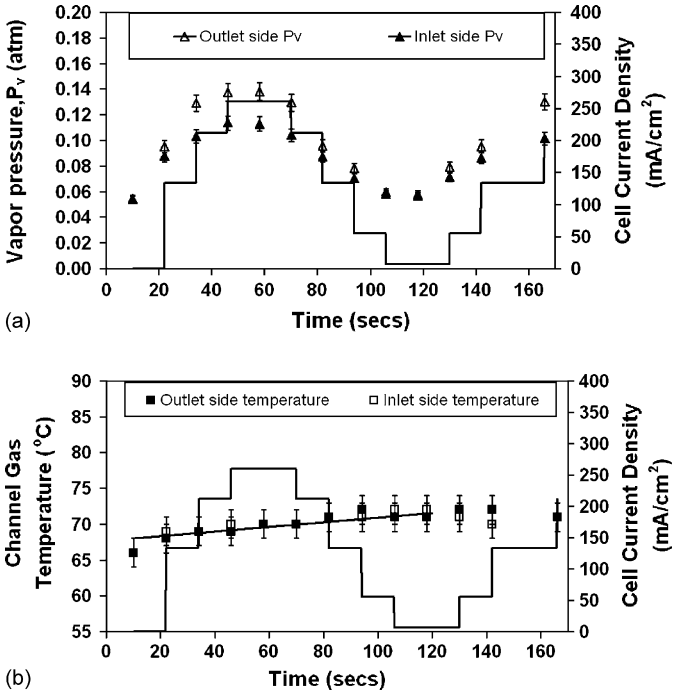

Fig. 11. Variation of (a) partial pressure and (b) temperature with dynamic load of low frequency for the two channels. Inlet partial pressure is 0.05 atm and the cell nominal temperature is 65 °C. Note that the amplitude of the current profile is twice than that of Fig. 7.

4. Conclusions

The measurements of water vapor partial pressure and temperature across two channels of the bipolar plate of a PEM fuel cell operating under steady and dynamic conditions were performed using a diagnostic technique based on tunable diode laser absorption spectroscopy. The technique is based on the measurements of water absorption characteristics that are sensitive to temperature and partial pressure in the operating range of a PEM fuel cell. The reported measurements are the first simultaneous non-intrusive water and temperature measurements made in two flow channels under steady and transient operation of the fuel cell.

For the steady-state measurements, simultaneous monitoring of two channels showed an increase in water vapor concentration between the inlet and outlet measurement channels, demonstrating a non-homogeneous distribution of species in the plane of the bipolar plate flow passages. The results showed a greater discrepancy in the inlet and outlet water content with increasing load of the fuel cell. The measured increase in water partial pressure near the inlet and the outlet channels of the serpentine flow path was found to be primarily due to the water production in between the two locations and electro-osmotic drag was found to be insignificant for the conditions examined. The temperature of the cell, which is regulated externally, showed no systematic variation between the two channels. However, other cell designs, operating conditions, or thermal boundary conditions will show different balances among the water production and transport processes and must be separately studied.

Measurements taken during two sinusoidal time varying current profiles showed the effects of frequency and amplitude of the dynamic load on the distribution of partial pressure and temperature in the two measurement channels. The water vapor partial pressure increases between inlet and outlet in a quasi-steady manner without any measurable phase shift with respect to the current profile. The non-homogeneous water distribution observed in the steady-state measurements, is equally apparent in the dynamic loading measurements. However, the temperature does not reach equilibrium during dynamic loading, even at frequencies as slow as $f = 1/120$ Hz.

The optical, non-intrusive measurement technique demonstrated in this study can be utilized for fundamental studies for better understanding of PEM fuel cell design and operation. It provides a diagnostic tool that is capable of interrogating local effects with good temporal resolution.

Acknowledgment

The research reported here was funded by the U.S. Army RDECOM, CERDEC (Fort Belvoir, VA) through the Connecticut Global Fuel Cell Center (CGFCC).

References

[1] J. Larminie, A. Dicks, Fuel Cell Systems Explained, Wiley, New York, 2000.
[2] P. Costamagna, S. Sirinivasan, J. Power Sources 102 (2001) 253–269.
[3] G. Alberti, M. Casciola, L. Massinelli, B. Bauer, J. Membr. Sci. 185 (2001) 73–81.
[4] M.L. Perry, J. Newman, E.J. Cairns, J. Electrochem. Soc. 145 (1998) 5–15.
[5] D.J. Beaubien, Sensors 2 (2005) 30–34.
[6] Q. Dong, J. Kull, M.M. Mench, J. Power Sources 139 (2005) 106–114.
[7] M.M. Mench, Q.L. Dong, C.Y. Wang, J. Power Sources 124 (2003) 90–98.
[8] I. Tkach, A. Panchenko, T. Kaz, V. Gogel, K.A. Friedrich, E. Roduner, Phys. Chem. Chem. Phys. 6 (2004) 5419–5426.
[9] D. Kramer, J. Zhang, R. Shimoi, E. Lehmann, A. Wokaun, K. Shinohara, G.G. Scherer, Electrochem. Acta 50 (2005) 2603–2614.
[10] R. Satija, D.L. Jacobson, M. Arif, S.A. Werner, J. Power Sources 129 (2004) 238–245.
[11] V.R. Albertini, B. Paci, A. Generosi, S. Panero, M.A. Navarra, M. di Michiel, Electrochem. Solid State Lett. 7 (2005) A519–A521.
[12] S. Basu, H. Xu, M.W. Renfro, B.M. Cetegen, ASME J. Fuel Cell Sci. Technol. 3 (2006) 1–7.
[13] S. Basu, G. Haluk, M.W. Renfro, B.M. Cetegen, J. Power Sources 159 (2006) 987–994.
[14] S.S. Penner, Quantitative Molecular Spectroscopy and Gas Emissivities, Addison-Wesley, 1959.